Engineering Geology 264 (2020) 105323

Contents lists available at ScienceDirect

Engineering Geology

journal homepage: www.elsevier.com/locate/enggeo

On an energy-based criterion for defining slope failure considering spatially varying soil properties

Linchong Huang[a], Shuai Huang[b], Zhengshou Lai[b,*]

[a] School of Aeronautics and Astronautics Engineering, Sun Yat-sen University, Guangzhou 510275, China
[b] School of Intelligent Systems Engineering, Sun Yat-sen University, Guangzhou 510275, China

ARTICLE INFO

Keywords:
Slope stability analysis
Energy characteristics
Random field
Finite difference method
Strength reduction method

ABSTRACT

The definition of slope failure is a critical issue for strength reduction method-based slope stability analysis. Conventional slope failure criteria, which rely heavily on the distributions of stress, strain and displacement throughout the slope, are relatively complicated and create ambiguity in practical applications. Recognizing such shortcomings, a new energy-based criterion for defining slope failure was recently developed in the literature. In this work, further analyses are performed to investigate the validity of this energy-based criterion for slope stability analysis in which spatially varying soil properties are considered. With the slope being modeled by the finite difference method, random field theory is adopted to generate cross-correlated soil strength properties for the slope. Then, the slope system is solved and analyzed with a consecutive series of strength reduction factors (SRFs). In particular, various forms of energy in the slope system are calculated with different SRFs, and the characteristics of the energy distribution and evolution with increasing SRFs are analyzed. The results indicate that the slope system exhibits a significant energy change when the SRF increases to a critical value, which is a good indicator of slope failure. The areas in the slope characterized by considerable energy dissipation present a profile that is very close to the profile of the critical slip surface of the slope. These findings regarding the characteristics of the energy distribution and energy evolution could be further utilized to develop more efficient approaches to determine factors of safety and critical slip surfaces.

1. Introduction

Originally introduced by Zienkiewicz et al. (1975), the finite element-based strength reduction method (FE-SRM) has been widely used for analyzing slope stability and evaluating factors of safety (FSs). The FE-SRM is applicable to complicated geometries and complex boundary and loading conditions; moreover, this technique can yield a variety of information, such as stress, strain and displacement, and can realistically describe soil behavior (Tu et al., 2016). In particular, when incorporated with appropriate searching algorithms, the FE-SRM is capable of locating the critical slip surface in an automatic fashion. Another similar method is the finite difference-based strength reduction method (FD-SRM), in which the finite difference method is adopted to solve the equivalent static problem. Many excellent FE-SRM or FD-SRM applications can be found in Zienkiewicz et al. (1975), Matsui and San (1992), Fu and Liao (2010), Huang and Jia (2009), Zhang et al. (2013).

In both the FE-SRM and the FD-SRM, a critical issue is the definition of slope failure, the condition at which the critical slip surface can be determined and the corresponding SRF is taken as the FS. Three conventional criteria that are commonly used to define slope failure are summarized in Tu et al. (2016), including the following: (1) the thorough propagation of the plastic zone, (2) a sudden increase in nodal displacements, and (3) the nonconvergence of FE or FD solvers. However, as noted by Tu et al. (2016), the metrics in these three criteria can be complicated and cause ambiguity in practical applications. The first criterion is subjective because the thorough propagation of the plastic zone is difficult to quantify. The second criterion is based on the fact that the sliding zone of a slope will exhibit large displacements if it loses its stability; for cases in which the sliding zone (or slip surface) is not known as a priori information, this criterion might not be effective because different locations can exhibit different magnitudes of displacements. The performance of the third criterion (i.e., the nonconvergence of FE or FD solvers) depends on the iteration and tolerance settings of the FE or FD solvers. Usually, a solution is considered to be nonconvergent if the solver cannot achieve the preset tolerance within the maximum number of iterations. This criterion could be computationally inefficient because the maximum iteration number is usually set to be relatively large. Additionally, this criterion lacks appropriate

* Corresponding author.
E-mail address: laizhengsh@mail.sysu.edu.cn (Z. Lai).

https://doi.org/10.1016/j.enggeo.2019.105323
Received 19 April 2019; Received in revised form 26 September 2019; Accepted 29 September 2019
Available online 31 October 2019
0013-7952/

physical meaning. Recognizing such shortcomings, Tu et al. (2016) studied the evolution of energy in a slope with increasing SRFs and developed a new slope failure criterion based on the energy evolution features. This energy-based criterion has been shown to be more accurate and physically meaningful than the conventional criteria.

The focus of this study is also on the energy-based criterion for defining slope failure, especially considering heterogeneous soil properties. Heterogeneous soil properties have long been recognized in geotechnical engineering. Soil heterogeneity can originate from two aspects (Kim, 2005; Chen et al., 2012): (1) inherent heterogeneity, which refers to natural fluctuations due to geological and environmental effects (e.g., variable soil constituents and preferred alignments during the transport and deposition of soil grains) (Phoon and Kulhawy, 1999; Elkateb et al., 2003; Chen et al., 2016; Liu et al., 2017), and (2) induced heterogeneity, which occurs as a result of physical phenomena (e.g., dilational deformation in shear bands or critical slip surfaces) that alter the characteristics of the soil medium (Sun et al., 2013; Ma and Wang, 2016). In this work, we consider only inherent heterogeneity.

Although soil properties vary in space, such variations are usually spatially correlated or dependent on each other. Thus far, random field theory has been shown to be an effective method for considering spatially varying but correlated soil properties. Many previous studies have considered random field soil properties in slope stability analysis. For example, Cho (2007, 2009) performed probabilistic slope stability analyses considering random field soil properties based on Monte Carlo simulation (MCS) with analytic (e.g., Spencer's method and the limit equilibrium method) or computational (e.g., the finite element method) slope analysis methods. Similarly, Hicks and Spencer (2010), Xiao et al. (2016) studied the influences of soil heterogeneity on the reliability and failure of slopes but from a 3D perspective. To account for prior knowledge (e.g., borehole measurements) or site-specific information (e.g., geological profiles) of soil properties and thus to avoid overestimating the variability, Kim and Sitar (2013), Liu et al. (2017a) proposed approaches to simulate conditional random fields that account for known data from field measurements; furthermore, Li et al. (2014), Deng et al. (2017), Zhou et al. (2018d) considered random field soil properties with linear trends, layered profiles, or embedded geological units in their slope stability analyses. Nevertheless, it is worth noting that probabilistic slope stability analyses with spatially varying soil properties usually involve numerous MCSs, which can be extremely time consuming. Several excellent studies have addressed this issue using various methods, including the responsive surface method (Li et al., 2015a), the bootstrap method (Li et al., 2015b), and the subset simulation technique (Jiang and Huang, 2016; Jiang et al., 2018).

In this work, slope stability analysis is performed using an FD-SRM model with cross-correlated soil properties that are simulated based on random field theory. In particular, the effects of spatially varying soil properties on the energy of the slope system (e.g., gravitational potential energy, elastic energy, dissipated energy, and kinetic energy) in terms of the spatial distribution and evolution of energy are investigated. The remainder of this paper is structured as follows. Section 2 briefly describes the FD-SRM model and the calculation of energy in the slope system, and Section 3 describes the random field model. Section 4 presents the numerical setup of an illustrative 2D slope problem using the FD-SRM. The simulation results and analyses are reported in Section 5, followed by some concluding remarks in Section 6.

2. The finite difference-based strength reduction method

2.1. Finite difference method

The finite difference method (FDM) is a well-established numerical method for solving differential equations in engineering mechanics. It is advantageous to model large-strain plastic collapse and flow problems using an explicit Lagrangian calculation scheme. Similar to the finite element method (FEM), the FDM also discretizes a continuous domain into an equivalent discrete mesh. However, in the FDM, the first-order space and time derivatives of a variable are approximated by finite differences while assuming linear variations of the variable over finite spatial and temporal intervals, respectively Itasca Consulting Group Inc (2012). All forces are assumed to be concentrated at the nodes, and the continuum-sense stress and its derivatives are transformed into forces at the nodes. As such, the balance of linear momentum for a static problem is equivalently solved in the FDM as the following discrete form of Newton's law at the nodes

$$\boldsymbol{m}\frac{\partial \boldsymbol{v}}{\partial t} = \boldsymbol{F}^{\sigma} + \boldsymbol{F}^{b} + \boldsymbol{F}^{d} \tag{1}$$

where $\boldsymbol{m}$ is the fictitious nodal mass; $\boldsymbol{v}$ is the nodal velocity; and $\boldsymbol{F}^{\sigma}$, $\boldsymbol{F}^{b}$, and $\boldsymbol{F}^{d}$ are the fictitious nodal forces associated with the stress, body force, and damping force, respectively. The nodal velocity and damping force vanish for an equivalent static problem when it reaches convergence. Details regarding the formulation of the FDM can be found in Forsythe and Wasow (1960), Smith (1985), Itasca Consulting Group Inc (2012).

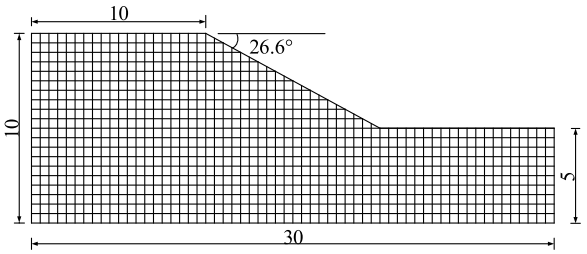

Fig. 1. Geometry and dimensions of the illustrative 2D slope (unit: m).

Table 1
Random field parameters for the soil strength properties. COV represents the coefficient of variation. The parameter $\rho_{c',\phi'}$ represents the cross-correlation between c' and ϕ'.

Property	Mean	COV	θ_x	θ_z	$\rho_{c',\phi'}$
c'	10 kPa	0.3	25 m	2.5 m	−0.5
ϕ'	15°	0.2	25 m	2.5 m	−0.5

2.2. Strength reduction method

In the strength reduction method (SRM), soil strength properties are iteratively and incrementally reduced by a consecutive series of strength reduction factors (SRFs) (Zienkiewicz et al., 1975; Fu and Liao, 2010). Then, the factor of safety (FS) is defined as the SRF, with which the slope fails. Considering the widely used Mohr-Coulomb material model, the shear strength τ_f is given by

$$\tau_f = c' + \sigma_n \tan\phi' \tag{2}$$

where c' and ϕ' are the effective cohesion and effective friction angle, respectively, and σ_n is the normal stress. By the SRM, the reduced strength properties are calculated as (Zienkiewicz et al., 1975; Tu et al., 2016)

$$c_r = \frac{1}{\mathrm{SRF}}c' \tag{3}$$

$$\phi_r = \arctan\left(\frac{1}{\mathrm{SRF}}\tan\phi'\right) \tag{4}$$

where c_r and ϕ_r are the reduced cohesion and reduced friction angle, respectively, and *SRF* represents the strength reduction factor.

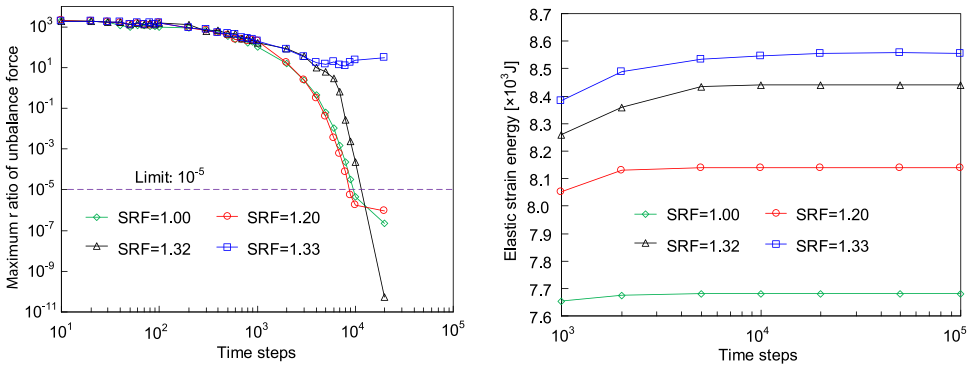

(a) Unbalanced force (b) Elastic strain energy

Fig. 2. Convergence profiles of the FD solver in terms of (a) the maximum ratio of unbalanced force and (b) elastic strain energy.

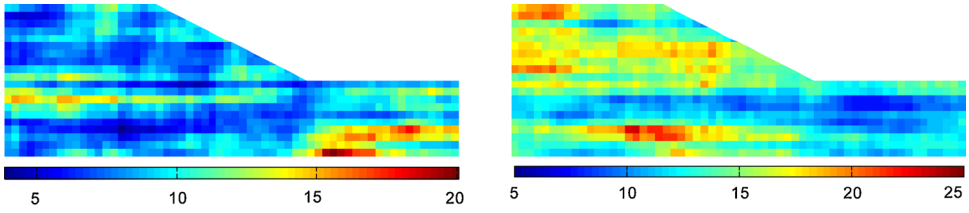

(a) Cohesion (b) Friction angle

Fig. 3. Example of the spatially varying soil strength properties: (a) cohesion (unit: kPa) and (b) friction angle (unit: °).

2.3. Calculation of energy

In this slope system, there are four forms of energy: (1) gravitational potential energy E^g, (2) elastic strain energy E^e, (3) dissipated energy E^d, and (4) kinetic energy E^k. Considering a slope as an isolated system, the work performed by gravity would first lead to an increase in elastic strain energy. Then, with the slope experiencing continuous deformation, some slope elements would yield and enter the plastic regime, in which part of the work performed by gravity would dissipate as a result of plastic deformation. Once the slope fails, the work performed by gravity is further converted into kinetic energy. The evolution of these forms of energy in this slope system obeys the law of conservation of energy, expressed as

$$\Delta(E^g + E^e + E^d + E^k) = 0 \tag{5}$$

where the symbol Δ indicates a change in energy. These different forms of energy are calculated as follows (Sloan, 2013; Tu et al., 2016)

$$E^g = \int_\Omega \rho g \Delta h \ \mathrm{d}\Omega \tag{6}$$

$$E^e = \int_\Omega \frac{1}{2}\boldsymbol{\sigma}: \boldsymbol{\varepsilon}^e \ \mathrm{d}\Omega \tag{7}$$

$$E^d = \int_\Omega \left(U^\sigma - \frac{1}{2}\boldsymbol{\sigma}: \boldsymbol{\varepsilon}^e\right)\mathrm{d}\Omega \tag{8}$$

$$E^k = \int_\Omega \frac{1}{2}\rho v^2 \ \mathrm{d}\Omega \tag{9}$$

where ρ is the soil density; g is the gravitational acceleration; Δh represents the height as a distance from a reference surface that is positive when one element is above the reference surface, and vice versa; $\boldsymbol{\sigma}$ and $\boldsymbol{\varepsilon}^e$ are the stress tensor and elastic strain tensor, respectively; U^σ is the total strain energy density, which can be calculated in integration form as $U^\sigma = \int \boldsymbol{\sigma} : \mathrm{d}\boldsymbol{\varepsilon}$; and v is the velocity. The symbol ':' denotes a double contraction of adjacent indices of a tensor of rank two or higher (e.g., $\boldsymbol{\sigma}: \boldsymbol{\varepsilon}^e = \sigma_{ij}\varepsilon^e_{ij}$).

3. Random field soil properties

With the slope modeled by the FDM, random field theory is used to generate the spatially varying yet correlated soil properties for the slope. By random field theory, a random field can be defined as a collection of random variables with each random variable being a function of some continuous domain parameter (e.g., the coordinates of each domain location). A general procedure for creating a random field of soil properties usually includes two major steps: (1) the field discretization step, in which a random field is discretized and approximated by a finite set of random variables, and (2) the field generation step, in which realizations of the discrete random variables are sampled from distribution models with the specified mean, variance, and spatial correlation.

The methods employed for the field discretization step can be divided into three groups: point discretization, average discretization, and series expansion methods. Reviews of several discretization methods can be found in Li and Der Kiureghian (1993), Ditlevsen (1996), Matthies et al. (1997). In this work, the midpoint method, which was first introduced by Der Kiureghian and Ke (1988), is adopted. The midpoint method approximates the random field in each mesh element by a single random variable, whose value is defined as the value of the field at the centroid of that element. After discretization, the random field is characterized by a vector of random variables that are correlated with each other. In this paper, the covariance matrix decomposition method is adopted to sample the correlated random variables because it is simple to implement and sufficiently accurate. The main concepts and procedures for simulating cross-correlated soil properties are briefly described as follows.

With reference to the covariance matrix decomposition method, the variables $\boldsymbol{Z}_{[n]}$, where n indicates the number of mesh elements, which follow a standard normal distribution, could be sampled from (Davis, 1987)

$$\boldsymbol{Z}_{[n]} = \boldsymbol{L}_{[n\times n]}\boldsymbol{U}_{[n]} \tag{10}$$

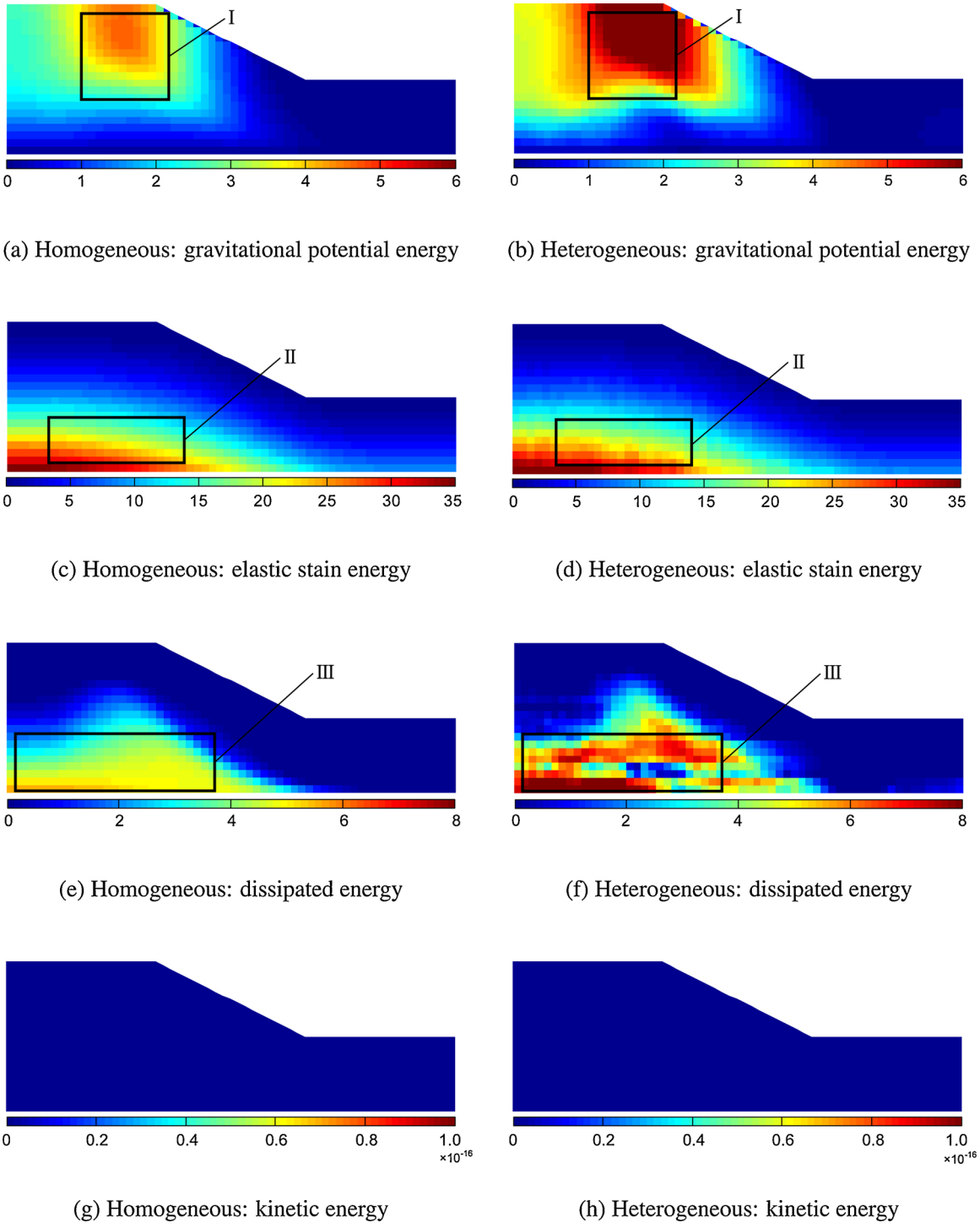

Fig. 4. Contours of different forms of energy in the slope when SRF = 1.0. Boxes I, II, and III highlight some elements that display significant energy changes when soil heterogeneity is introduced (unit: J).

where $\boldsymbol{U}_{[n]}$ is a vector of independent random variables obeying a standard normal distribution and $\boldsymbol{L}_{[n\times n]}$ is the Cholesky decomposition of the correlation matrix $\boldsymbol{C}_{[n\times n]}$ satisfying $\boldsymbol{C} = \boldsymbol{L}\boldsymbol{L}^T$. The correlation matrix $\boldsymbol{C}$ consists of components ρ_{ij}, which characterize the correlation between the standard-normalized soil property within the ith soil element and that within the jth element. In this work, a single exponential function (Li et al., 2015a) is adopted to describe the spatial autocorrelation structure of soil, and this function is written as

$$\rho(\tau_x, \tau_z) = \exp\left[-2\left(\frac{\tau_x}{\theta_x} + \frac{\tau_z}{\theta_z}\right)\right] \tag{11}$$

where τ_x and τ_z are the horizontal and vertical distances between two points, respectively, and θ_x and θ_z represent the horizontal and vertical scales of fluctuation (i.e., the correlation lengths), respectively. Then, based on the sampling strategy of a single soil property, multivariate cross-correlated soil properties can be obtained as (Cho and Park, 2010; Deng et al., 2017)

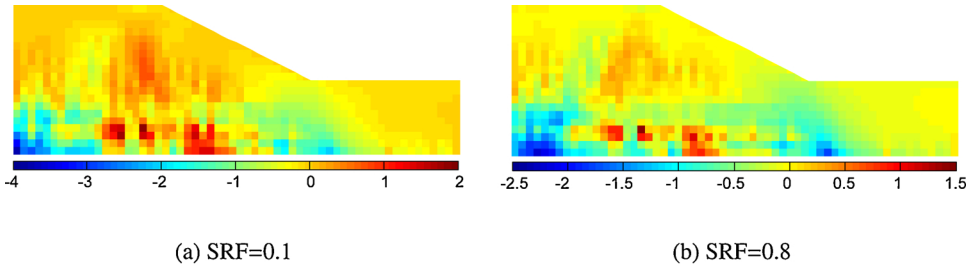

(a) SRF=0.1 (b) SRF=0.8

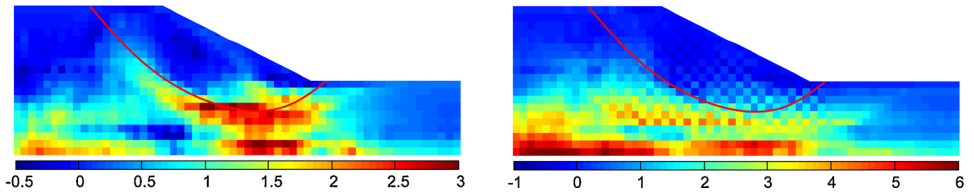

(c) SRF=1.32 (d) SRF=2.0

Fig. 5. Change in the elastic strain energy in each element for different SRFs with respect to the no-reduction case: (a) SRF = 0.1, (b) SRF = 0.8, (c) SRF = 1.32 (i.e., SRF = FS), and (d) SRF = 2.0. The solid red line in (c) and (d) represents the critical slip surface that is obtained from FLAC3D. (For interpretation of the references to color in this figure legend, the reader is referred to the web version of this article.)

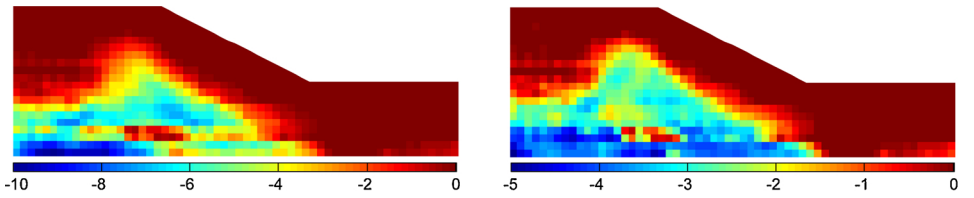

(a) SRF=0.1 (b) SRF=0.8

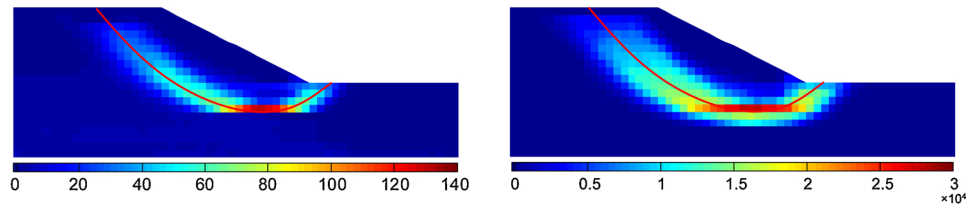

(c) SRF=1.32 (d) SRF=2.0

Fig. 6. Change in the dissipated energy in each element for different SRFs with respect to the no-reduction case: (a) SRF = 0.1, (b) SRF = 0.8, (c) SRF = 1.32 (i.e., SRF = FS), and (d) SRF = 2.0. The solid red line in (c) and (d) represents the critical slip surface that is obtained from FLAC3D. (For interpretation of the references to color in this figure legend, the reader is referred to the web version of this article.)

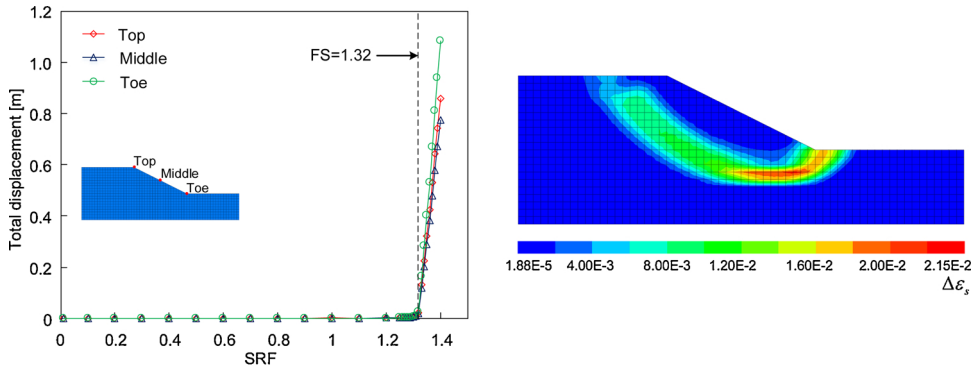

(a) Nodal displacement (b) Shear strain increments

Fig. 7. Definition of slope failure based on (a) the nodal displacement and (b) the propagation of the plastic zone through the slope visualized from the shear strain increments.

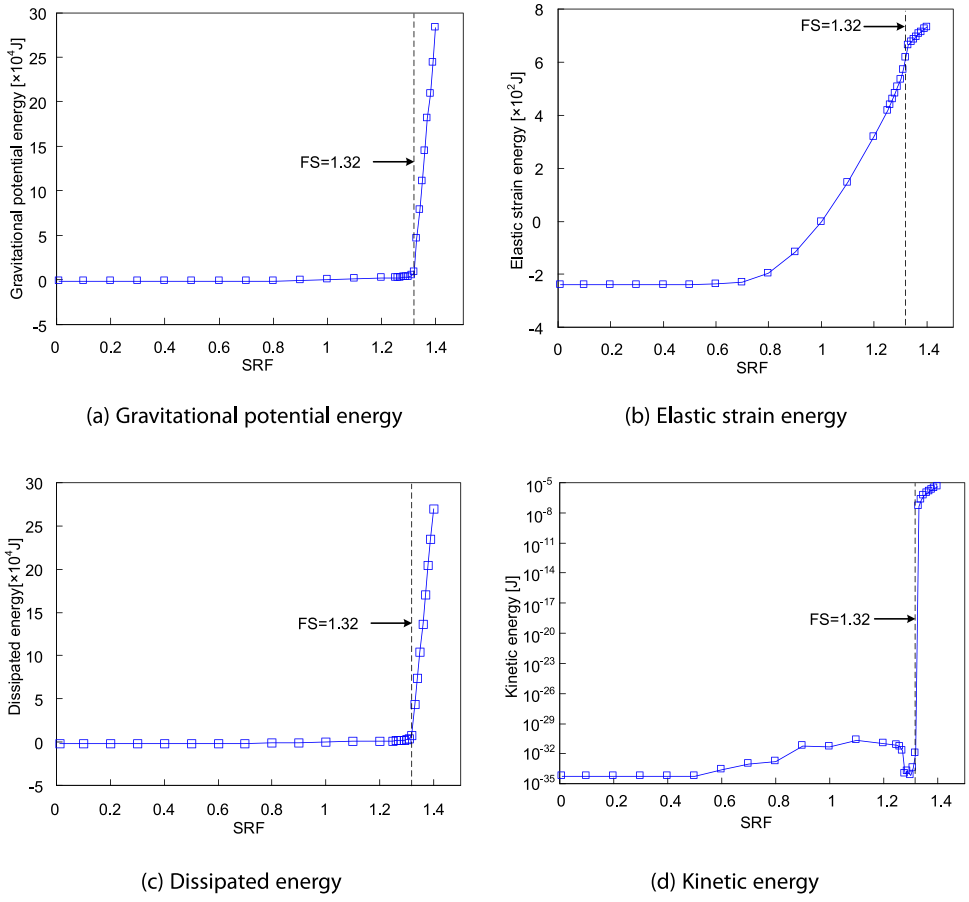

Fig. 8. Evolution of the change in energy integrated over the entire slope (with respect to the reference case, i.e., SRF = 1.0) for different SRFs: (a) gravitational potential energy, (b) elastic strain energy, (c) dissipated energy, and (d) kinetic energy.

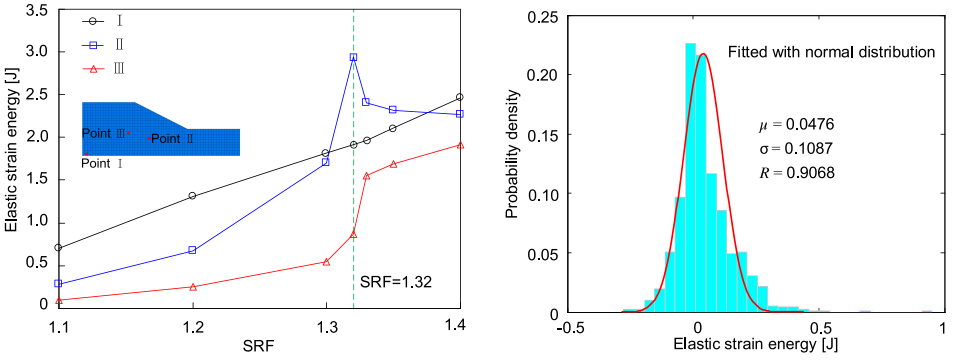

Fig. 9. (a) Evolution of the elastic strain energy change (with respect to the reference case where SRF = 1.0) at probed locations and (b) the histogram of elastic strain energy change of all elements. SRF = 1.32 is the value of the FS.

$$\boldsymbol{X}_{[n\times m]} = [\boldsymbol{X}_n^1, \boldsymbol{X}_n^2, \ldots, \boldsymbol{X}_n^m] = [\boldsymbol{Z}_n^1, \boldsymbol{Z}_n^2, \ldots, \boldsymbol{Z}_n^m](\boldsymbol{L}_{[m\times m]}^R)^T \tag{12}$$

where $\boldsymbol{X}_{[n\times m]}$ represents the cross-correlated soil properties with n indicating the number of mesh elements and m indicating the number of soil properties and $\boldsymbol{L}^R$ represents the lower Cholesky decomposition of the cross-correlation matrix $\boldsymbol{R}$ such that each component R_{ij} represents the cross-correlation between the soil properties X^i and X^j.

Insomuch that soil properties are log normally distributed, the final soil properties $\boldsymbol{S}$ could be obtained from variables $\boldsymbol{X}$ following a standard normal distribution via a transformation (Gong et al., 2018) as

$$\boldsymbol{S} = \exp(\mu_{\ln s} + \sigma_{\ln s}\boldsymbol{X}) \tag{13}$$

where $\mu_{\ln s}$ and $\sigma_{\ln s}$ are the mean and standard deviation, respectively, of the logarithmic variable $\boldsymbol{S}$ (i.e., $\ln \boldsymbol{S}$) such that

$$\sigma_{\ln s} = \sqrt{\ln[1 + (\sigma_s/\mu_s)^2]} \tag{14}$$

$$\mu_{\ln s} = \ln \mu_s - \frac{1}{2}\sigma_{\ln s}^2 \tag{15}$$

where μ_s and σ_s are the mean and standard deviation of variable $\boldsymbol{S}$, respectively.

It is worth mentioning that the procedures described herein provide a general approach to generate cross-correlated soil properties, although this approach is effective at a single scale (i.e., the sizes of the

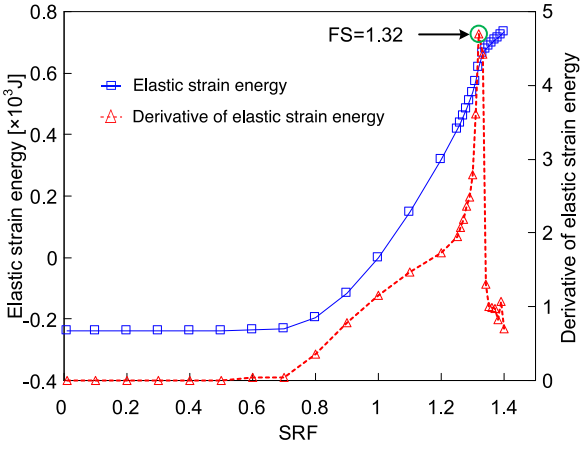

Fig. 10. Derivative of the elastic strain energy change with respect to the SRF.

domain elements should be compatible without large differences in their order of magnitude). For cases in which finer meshes are required (e.g., in the vicinity of a slip surface or in regions with special interests) for achieving a higher modeling accuracy, multiscale random field models are necessary to consistently represent fine- and coarse-scale random fields while maintaining appropriate spatial correlation structures across scales. Interested readers are referred to Chen et al. (2015, 2016) for a detailed description of the appropriate methods.

4. Illustrative example

4.1. Model setup

To investigate the effects of spatially varying soil properties on the energy distribution and evolution in slope stability analysis, a 2D slope with a height of 10 m and a slope angle of 26.6° is studied as an illustrative example. The slope geometry is shown in Fig. 1. The soil in the slope is idealized as a Mohr-Coulomb elastic-perfectly plastic material, and the material properties are specified as follows: unit weight $\gamma = 20\ \mathrm{kN/m^3}$, Young's modulus $E = 100\ \mathrm{MPa}$, and Poisson's ratio $\nu = 0.3$. The strength properties c' and ϕ' are assumed to be lognormally distributed with an anisotropic exponential autocorrelation structure and to be negatively cross-correlated with each other (see Section 3). Note that the spatial variability of the deformation properties, Young's modulus and Poisson's ratio, is not considered in this work because their variations are found to be relatively low compared with the variations of the strength properties (i.e., cohesion and friction angle) (Duncan, 2000; Jiang et al., 2014). Additionally, as noted by Griffiths and Marquez (2007), Poisson's ratio has minimal influence on the calculated FS in slope stability analysis. The random field parameters for the strength properties are summarized in Table 1.

FLAC3D software (Itasca Consulting Group Inc, 2012) is adopted to simulate this example slope problem. The 2D slope is modeled in 3D with a small thickness of 1 m normal to the 2D model. Regular brick elements with a size of 0.5 m are used to discretize the slope domain for the random field simulation and FD solution. The soil elements along the slope surface taper into wedges. For the boundary conditions, the bottom of the slope is fixed, while the lateral sides are constrained with zero horizontal displacements, and the slope surface is kept free. The random field soil strength properties are first generated in MATLAB and

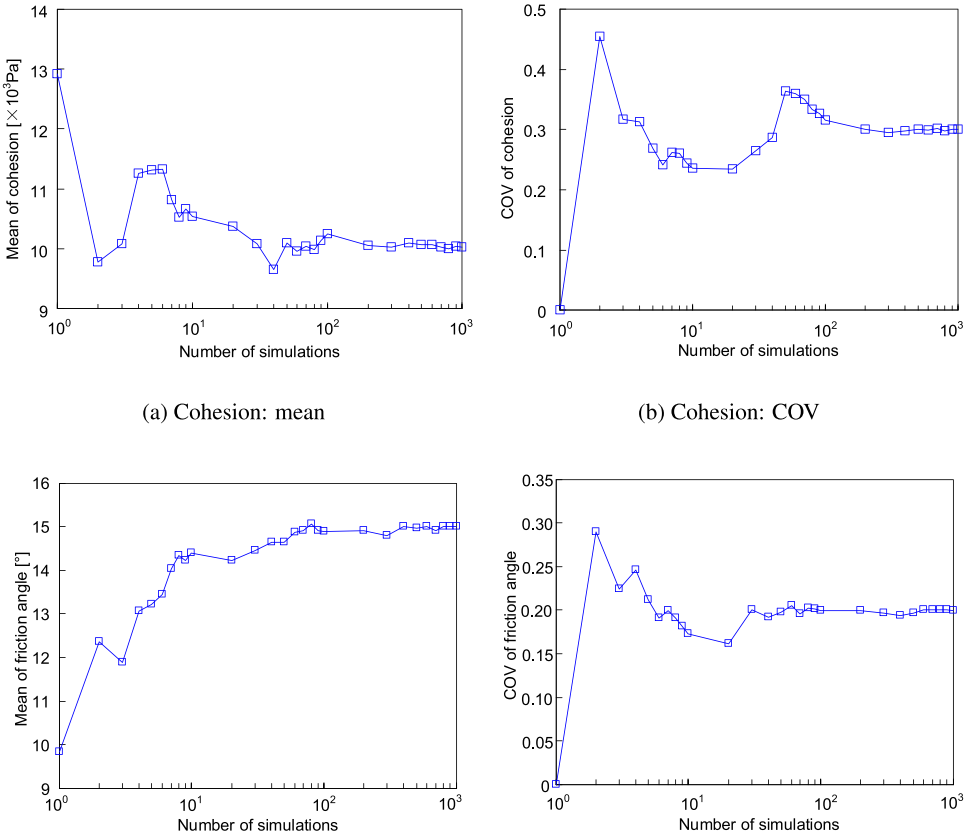

(a) Cohesion: mean (b) Cohesion: COV

(c) Friction angle: mean (d) Friction angle: COV

Fig. 11. Statistics of the soil cohesion and friction angle at a randomly probed location.

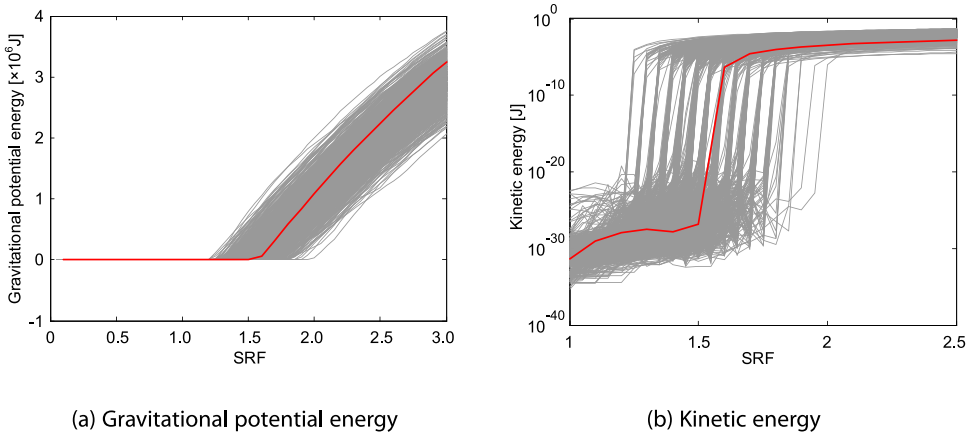

Fig. 12. Evolution of (a) the gravitational potential energy change and (b) the kinetic energy change over 1000 MCSs. The solid red line represents the result of the homogeneous case. (For interpretation of the references to color in this figure legend, the reader is referred to the web version of this article.)

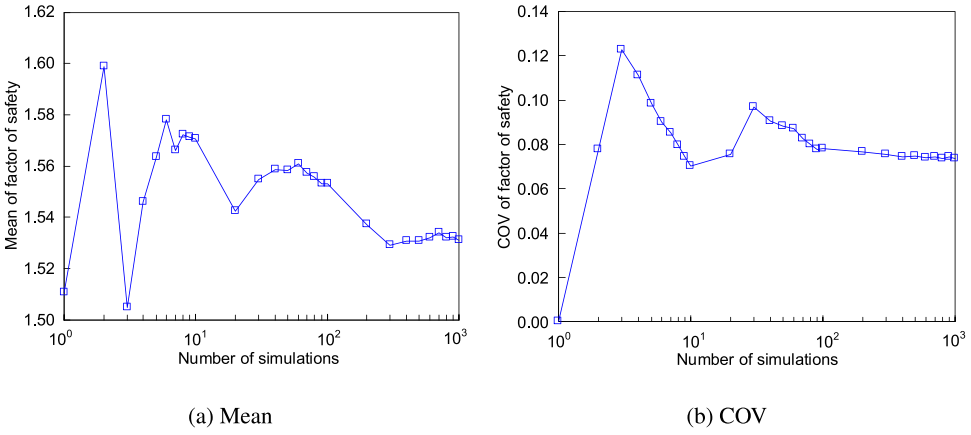

Fig. 13. FS statistics as a function of the number of MCSs: (a) mean and (b) COV.

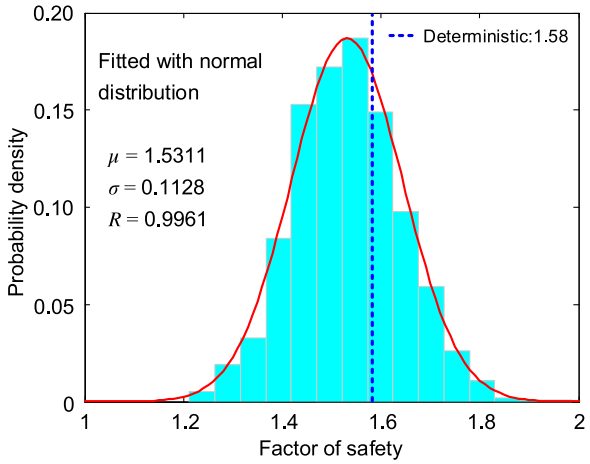

Fig. 14. Histogram of the FS based on the 1000 MCSs. The mean FS is approximately 1.53, and the COV is approximately 0.07. The FS of the homogeneous case is approximately 1.58.

are then saved and imported into FLAC3D as external text files.

4.2. Convergence characteristics

Before performing a probabilistic slope stability analysis, it is necessary to verify the convergence characteristics of the FD solver. In the FDM, the solution is deemed to successfully converge if the maximum value of the ratio of the unbalanced force at a gridpoint to the mean of the set of absolute forces acting at the gridpoint (simplified as the ratio of unbalanced force hereafter) is below a desired tolerance (Itasca Consulting Group Inc, 2012). A solution can fail to converge due to two situations: (1) slope failure occurs (a *true* nonconvergent situation), and (2) an insufficient number of iterations (a *fake* nonconvergent situation). Specifying a large iteration number could avoid *fake* nonconvergent situations but would also increase the computational cost. To obtain an optimal iteration number, the evolution of the ratio of unbalanced force with the iteration number is studied, and the results are plotted in Fig. 2a. In this test, the results are obtained from one random realization of a heterogeneous soil field. The results of the cases with different SRFs indicate that 20,000 is a reasonable number of iterations for this example problem. For the same purpose, the evolution of the elastic strain energy as a function of the iteration number is plotted in Fig. 2b. It is observed that the elastic strain energy tends to constant values within 20,000 iterations for all different SRFs (e.g., either convergent or nonconvergent situations).

5. Results and analyses

5.1. Spatial distributions of the various forms of energy

We start this section by presenting the results of the spatial distributions of the various forms of energy in the slope system. Two cases, one with homogeneous soils and another with heterogeneous soils, are considered for comparison purposes. With the random field parameters listed in Table 1, an example of the spatially varying and cross-

correlated soil strength properties generated based on random field theory is shown in Fig. 3. These two contours exhibit layer-like profiles, which is consistent with the fact that a greater scale of fluctuation is specified in the horizontal direction. By comparing these two contours, the negative cross-correlation relationship between the cohesion and the friction angle can be clearly identified.

With this example of soil strength properties, the slope is analyzed using the FD-SRM model. Contours of the various forms of energy when the SRF equals 1.0 are shown in Fig. 4, where the same contours in the homogeneous case are also presented for comparison. Overall, the same type of energy in the homogeneous case and the heterogeneous case exhibits a similar profile. However, upon examining some elements more closely (see the highlighted areas I, II, and III in Fig. 4), it can be observed that soil heterogeneity changes the magnitude of the energy in these elements. Nevertheless, the kinetic energy is almost zero in both the homogeneous case (Fig. 4g) and the heterogeneous case (Fig. 4h) because the slope is in static equilibrium.

To gain insights into the characteristics of the energy evolution at each position when the SRF increases, the energy contours simulated with different SRFs are compared. Here, only the results of the elastic strain energy and the dissipated energy will be presented, as these two forms of energy are directly related to the stress and strain states of the slope. To better visualize the differences in the energy distribution between the cases with different SRFs, the energy change between the case with reduced strength properties and the case with no strength reduction (i.e., SRF = 1.0) is calculated. The change in the elastic strain energy is displayed in Fig. 5. No particular patterns can be identified among these contours. Specifically, some elements present an increase in the elastic energy (i.e., positive values), while the others present a decrease (i.e., negative values). Elements in the vicinity of the critical slip surface exhibit greater magnitudes of variation in the elastic strain energy.

Similarly, the change in the dissipated energy with different SRFs is shown in Fig. 6. In this case, most elements experience increasing energy dissipation as the SRF increases. For the cases with an SRF smaller than 1.0, the change in the dissipated energy is negative, indicating that the dissipated energy in the cases with an SRF smaller than 1.0 is smaller than that of the reference case (i.e., when the SRF equals 1.0). Then, when the SRF exceeds 1.32 (i.e., the value of the FS), the dissipated energy increases significantly. The elements with large magnitudes of dissipated energy present a profile that is quite similar to the profile of the critical slip surface. While the determination of the critical slip surface in slope stability analysis is a non-trivial task, the contour of dissipated energy could provide useful clues to obtain an initial estimate of the critical slip surface.

5.2. Energy-based criterion of slope failure

In this section, we investigate the validity of the energy-based criterion for defining slope failure in consideration of spatially varying soil properties. First, the FS results determined from the three conventional criteria are presented. For this example problem, the simulation is considered to be nonconvergent when the maximum ratio of unbalanced force does not reduce to 10^{-5} within 20,000 iterations Section 4.2). The results of the maximum ratio of unbalanced force for several different SRFs can be recalled from Fig. 2a. The maximum ratio of unbalanced force decreases to 10^{-5} in a quadratic manner within 20,000 iterations for the cases with SRFs smaller than the FS; for the cases with SRFs greater than the FS, the maximum ratio of unbalanced force vibrates around a large value as the iterations continue. According to the nonconvergence criterion of slope failure, the FS is determined to be approximately 1.32. Then, for the nodal displacement criterion, three nodes that are located at the top, the middle and the toe of the slope surface are probed (see the embedded figure in Fig. 7a). The total displacements of these three nodes are small for small SRFs, but they exhibit a sudden increase when the SRF increases to 1.32 (i.e., the FS). The value of the FS determined based on the nodal displacement criterion is consistent with that determined based on the nonconvergence criterion. Finally, Fig. 7b shows the results of the maximum shear strain increments. The elements with large shear strain increments present a clear pattern that propagates from the toe of the slope to the top of the slope. However, the propagation of the plastic zone through the slope is difficult to quantify and thus is not an efficient criterion for identifying slope failure.

To verify the energy-based criterion for defining slope failure, the evolution of each different form of energy in the slope system (i.e., gravitational potential energy, elastic strain energy, dissipated energy, and kinetic energy) with the SRF is plotted in Fig. 8. In these plots, the *y*-axis represents the energy change between the case with reduced strength properties and the reference case (i.e., the original model without strength reduction). The energy change results are integrated over the entire slope. For gravitational potential energy, dissipated energy, and kinetic energy, the energy change is nearly zero at the beginning and then exhibits a sudden increase when the SRF increases to the same critical value. This critical SRF is consistent with the FS value determined from the nonconvergence criterion. As such, the sudden change in each of these three forms of energy acts as a perfect indicator of slope failure. Compared with the conventional failure criteria, this new energy-based criterion treats the slope as a unit to calculate the energy change, and it provides a more physically meaningful explanation of slope failure (recalling the discussion in Section 2.3).

In slight contrast, the elastic stain energy continues to increase for all SRFs, which is different from the observations (i.e., the elastic stain energy increases and then decreases once the slope fails) made in Tu et al. (2016) for homogeneous slopes. In fact, the effects of a strength reduction on the elastic strain energy originate from two aspects. On the one hand, a slope with a higher SRF value tends to be *weaker* and experiences an overall larger extent of vertical displacement under the influence of gravity. As such, the elastic strain energy tends to increase due to the extra work performed by gravity. On the other hand, an increasing SRF means a decreasing soil strength, which reduces the capability of each element in the slope to store elastic strain energy. As a consequence, the elastic strain energy tends to decrease. These two effects counteract each other, leading the elastic strain energy to exhibit a generally complicated evolution profile. To conduct a more quantitative investigation into the evolution of the elastic strain energy, the energy changes (with respect to the reference case where SRF = 1.0) of several elements with different SRFs are plotted in Fig. 9a. These three plots represent the three different outcomes of the counteraction between the two effects mentioned above. As shown in this figure, point I exhibits a stable increasing profile for all SRFs, while point II exhibits a sudden decrease once the SRF becomes greater than the FS, and point III exhibits a sudden increase. A histogram of the elastic strain energy change in each element when the SRF increases from 1.32 (i.e., the value of the FS) to 1.33 is shown in Fig. 9b. The results clearly indicate that some elements exhibit an increase in the energy change, while the remainder exhibit a decrease. The probability density profile is slightly skewed to the positive side, indicating an overall increase in the elastic strain energy change.

However, we anticipate that because slope failure results in sudden changes in the gravitational potential energy, dissipated energy and kinetic energy, there would also be sudden changes in the elastic strain energy. In this regard, we calculate the derivative of the elastic strain energy change with respect to the SRF and plot the result in Fig. 10. The point with the maximum derivative of the energy change coincides with the point of slope failure (i.e., the point when the SRF is equal to the FS). Based on the results presented in this section, it is found that the energy-based criterion for defining slope failure is applicable to slopes with spatially varying soil properties.

5.3. Validation with Monte Carlo simulations

The validity of the energy-based criterion for defining slope failure is further demonstrated by a series of Monte Carlo simulations (MCSs). For a probabilistic slope stability analysis considering random field soil properties, MCSs are usually required to approach a statistical characterization of the slope stability. In this regard, we generate 1000 realizations of random field soil strength properties. With the results of 1000 MCSs, the statistics (i.e., the mean and COV) of the soil strength properties can be computed. Fig. 11 presented the mean and coefficient of variation (COV) of the soil cohesion and friction angle against the number of MCSs. The statistics of both the cohesion and the friction angle approach the prior specified values within 1000 MCSs. As such, 1000 Monte Carlo realizations are sufficient for this given example problem, and the results of these 1000 MCSs will be used in the following FD-SRM simulations.

The 1000 realizations of the random field soil strength properties are imported into the FD-SRM model, and the slope stability problem is solved. The energy evolution results for the 1000 MCSs are plotted in Fig. 12. Here, only the results of the gravitational potential energy and the kinetic energy are presented, as the profiles of the dissipated energy are quite similar to those of the gravitational potential energy, and the elastic strain energy has a typical profile that is not distinguishable when 1000 curves are plotted altogether (as shown in Fig. 10). Without exception, all energy evolution plots present similar profiles to those plots that have been shown and discussed in Fig. 8.

With the results of 1000 MCSs, the statistics of the FS can be analyzed. The evolution of the FS statistics with the number of MCSs is shown in Fig. 13. The mean and COV of the FS present large fluctuations for a small number of MCSs. With an increasing number of MCSs, the mean and COV gradually begin to stabilize and asymptotically approach a constant value. These results indicate that 1000 MCSs are sufficient to ensure the convergence of the FS statistics and are representative of this example. The histogram of the 1000 FSs is presented in Fig. 14. The results show that the 1000 FSs can be suitably fitted by a normal distribution with a mean at approximately 1.53 and a COV at approximately 0.07. The mean FS evaluated from the probabilistic slope stability analysis considering heterogeneous soil properties is slightly smaller than that evaluated from the deterministic analysis (e.g., 1.58) considering homogeneous soil properties.

6. Conclusions

In this work, the distributions and evolution of different forms of energy in a slope system are investigated using an FD-SRM model with random field soil strength properties. The equivalent static problem of a 2D slope is solved within a finite difference model, in which cross-correlated soil strength properties are considered and generated based on random field theory. The validity of the energy-based criterion for defining slope failure in the case of heterogeneous soil is demonstrated, and the effects of spatially varying soil strength properties on the energy distribution and evolution are discussed in depth. The main findings of this work are as follows:

1. The energy contours of the homogeneous model and the heterogeneous model exhibit quite similar patterns, and soil heterogeneity results in a slight difference in the magnitudes of the energy at each position.
2. With increasing SRFs, distinct changes in the elastic strain energy are observed insomuch that only some elements have an increasing elastic energy; the dissipated energy in each element continues to increase almost all the time, and the elements close to the critical slip surface exhibit a notably greater amount of energy dissipation than those at other positions.
3. The gravitational potential energy, dissipated energy, and kinetic energy all suddenly increase once the SRF increases and reaches a critical value (i.e., the value of the FS). Such an evolutionary feature of energy serves as a good indicator of slope failure, which is consistent with the failure condition defined by the nonconvergence criterion or the nodal displacement criterion.
4. The elastic stain energy continues to grow with an increasing SRF, while the derivative of the elastic strain energy with respect to the SRF reaches a maximum when the SRF is equal to the FS. This characteristic could also be used to define slope failure.
5. The statistics of soil properties and the FS could converge to constant values within 1000 MCSs; additionally, as calculated from probabilistic slope stability analysis, the mean FS is slightly smaller than that calculated from the homogeneous case.

Finally, it should be noted that while this energy-based method is useful for calculating the FS of a slope, it cannot obtain the exact slip surface when the slope fails. A good alternative for determining slip surfaces is to use the phase field model (Zhou et al., 2018a,b,c, 2019), which is also an energy-based method. The phase field model can obtain an obvious failure surface; hence, the application of this model constitutes one of our future research prospects.

Conflicts of interest

The authors declare no conflicts of interest.

Acknowledgements

This work was supported by the National Natural Science Foundation of China (Project No. 51678578), the Guangdong Natural Science Foundation (Project No. 2016A030313233), and the Guangzhou Science & Technology Program (Project No. 201704020139). This financial support is gratefully acknowledged. The authors are also grateful to the editor and reviewers for their helpful comments and suggestions.

References

Chen, Q., Seifried, A., Andrade, J.-E., Baker, J.-W., 2012. Characterization of random fields and their impact on the mechanics of geosystems at multiple scales. Int. J. Numer. Anal. Methods Geomech. 36 (2), 140–165.
Chen, Q., Wang, C., Juang, C.H., 2015. CPT-based evaluation of liquefaction potential accounting for soil spatial variability at multiple scales. J. Geotech. Geoenviron. Eng. 142 (2), 04015077.
Chen, Q., Wang, C., Juang, C.-H., 2016. Probabilistic and spatial assessment of liquefaction-induced settlements through multiscale random field models. Eng. Geol. 211, 135–149.
Cho, S.-E., 2007. Effects of spatial variability of soil properties on slope stability. Eng. Geol. 92 (3–4), 97–109.
Cho, S.-E., 2009. Probabilistic assessment of slope stability that considers the spatial variability of soil properties. J. Geotech. Geoenviron. Eng. 136 (7), 975–984.
Cho, S.-E., Park, H.-C., 2010. Effect of spatial variability of cross-correlated soil properties on bearing capacity of strip footing. Int. J. Numer. Anal. Methods Geomech. 34 (1), 1–26.
Davis, M.-W., 1987. Production of conditional simulations via the LU triangular decomposition of the covariance matrix. Math. Geol. 19 (2), 91–98.
Deng, Z.-P., Li, D.-Q., Qi, X.-H., Cao, Z.-J., Phoon, K.-K., 2017. Reliability evaluation of slope considering geological uncertainty and inherent variability of soil parameters. Comput. Geotech. 92, 121–131.
Der Kiureghian, A., Ke, J.-B., 1988. The stochastic finite element method in structural reliability. Probab. Eng. Mech. 3 (2), 83–91.
Ditlevsen, O., 1996. Dimension reduction and discretization in stochastic problems by regression method. Math. Models Struct. Reliab. Anal. CRC Math. Model. Ser. 2, 51–138.
Duncan, J.-M., 2000. Factors of safety and reliability in geotechnical engineering. J. Geotech. Geoenviron. Eng. 126 (4), 307–316.
Elkateb, T., Chalaturnyk, R., Robertson, P.-K., 2003. An overview of soil heterogeneity: quantification and implications on geotechnical field problems. Can. Geotech. J. 40 (1), 1–15.
Forsythe, G., Wasow, W.-R., 1960. Finite-Difference Methods for Partial Differential Equations, Applied Mathematical Series. Wiley, New York.
Fu, W., Liao, Y., 2010. Non-linear shear strength reduction technique in slope stability calculation. Comput. Geotech. 37 (3), 288–298.
Gong, W., Juang, C.-H., Martin II, J.-R., Tang, H., Wang, Q., Huang, H., 2018. Probabilistic analysis of tunnel longitudinal performance based upon conditional

random field simulation of soil properties. Tunn. Undergr. Space Technol. 73, 1–14.
Griffiths, D.-V., Marquez, R.-M., 2007. Three-dimensional slope stability analysis by elasto-plastic finite elements. Géotechnique 57 (6), 537–546.
Hicks, M.-A., Spencer, W.-A., 2010. Influence of heterogeneity on the reliability and failure of a long 3D slope. Comput. Geotech. 37 (7–8), 948–955.
Huang, M., Jia, C.-Q., 2009. Strength reduction FEM in stability analysis of soil slopes subjected to transient unsaturated seepage. Comput. Geotech. 36 (1–2), 93–101.
Itasca Consulting Group Inc, 2012. Fast Lagrangian Analysis of Continua in 3 Dimensions (FLAC 3D): User's Guide. Ver. 5.0. Itasca, Minneapolis.
Jiang, S.-H., Huang, J., Huang, F., Yang, J., Yao, C., Zhou, C.-B., 2018. Modelling of spatial variability of soil undrained shear strength by conditional random fields for slope reliability analysis. Appl. Math. Modell. 63, 374–389.
Jiang, S.-H., Li, D.-Q., Zhang, L.-M., Zhou, C.-B., 2014. Slope reliability analysis considering spatially variable shear strength parameters using a non-intrusive stochastic finite element method. Eng. Geol. 168, 120–128.
Jiang, S.H., Huang, J.-S., 2016. Efficient slope reliability analysis at low-probability levels in spatially variable soils. Comput. Geotech. 75, 18–27.
Kim, H., 2005. Spatial Variability in Soils: Stiffness and Strength. PhD Thesis. Georgia Institute of Technology.
Kim, J.M., Sitar, N., 2013. Reliability approach to slope stability analysis with spatially correlated soilproperties. Soils Found. 53 (1), 1–10.
Li, C., Der Kiureghian, A., 1993. Optimal discretization of random fields. J. Eng. Mech. 119 (6), 1136–1154.
Li, D.-Q., Qi, X.-H., Phoon, K.-K., Zhang, L.-M., Zhou, C.-B., 2014. Effect of spatially variable shear strength parameters with linearly increasing mean trend on reliability of infinite slopes. Struct. Saf. 49, 45–55.
Li, D.-Q., Jiang, S.-H., Cao, Z.-J., Zhou, W., Zhou, C.-B., Zhang, L.-M., 2015a. A multiple response-surface method for slope reliability analysis considering spatial variability of soil properties. Eng. Geol. 187, 60–72.
Li, D.-Q., Tang, X.-S., Phoon, K.-K., 2015b. Bootstrap method for characterizing the effect of uncertainty in shear strength parameters on slope reliability. Reliab. Eng. Syst. Saf. 140, 99–106.
Liu, W., Chen, Q., Wang, C., Juang, C.-H., Chen, G., 2017. Spatially correlated multiscale Vs30 mapping and a case study of the Suzhou site. Eng. Geol. 220, 110–122.
Ma, J., Wang, J., 2016. A stress-induced permeability evolution model for fissured porous media. Rock Mech. Rock Eng. 49 (2), 477–485.
Matsui, T., San, K.-C., 1992. Finite element slope stability analysis by shear strength reduction technique. Soils Found. 32 (1), 59–70.
Matthies, H.-G., Brenner, C.-E., Bucher, C.-G., Soares, C.-G., 1997. Uncertainties in probabilistic numerical analysis of structures and solids-stochastic finite elements. Struct. Saf. 19 (3), 283–336.
Phoon, K., Kulhawy, F.H., 1999. Evaluation of geotechnical property variability. Can. Geotech. J. 36 (4), 625–639.
Sloan, S.-W., 2013. Geotechnical stability analysis. Géotechnique 63 (7), 531.
Smith, G., 1985. Numerical Solution of Partial Differential Equations: Finite Difference Methods. Oxford University Press.
Sun, W.-C., Kuhn, M.-R., Rudnicki, J.-W., 2013. A multiscale DEM-LBM analysis on permeability evolutions inside a dilatant shear band. Acta Geotech. 8 (5), 465–480.
Tu, Y., Liu, X., Zhong, Z., Li, Y., 2016. New criteria for defining slope failure using the strength reduction method. Eng. Geol. 212, 63–71.
Zhang, Y., Chen, G., Zheng, L., Li, Y., Zhuang, X., 2013. Effects of geometries on three-dimensional slope stability. Can. Geotech. J. 50 (3), 233–249.
Zhou, S., Rabczuk, T., Zhuang, X., 2018a. Phase field modeling of quasi-static and dynamic crack propagation: COMSOL implementation and case studies. Adv. Eng. Softw. 122, 31–49.
Zhou, S., Zhuang, X., Rabczuk, T., 2018b. A phase-field modeling approach of fracture propagation in poroelastic media. Eng. Geol. 240, 189–203.
Zhou, S., Zhuang, X., Zhu, H., Rabczuk, T., 2018c. Phase field modelling of crack propagation, branching and coalescence in rocks. Theor. Appl. Fract. Mech. 96, 174–192.
Zhou, X.-P., Zhu, B.-Z., Juang, C.-H., Wong, L.-N.-Y., 2018d. A stability analysis of a layered-soil slope based on random field. Bull. Eng. Geol. Environ. 1–15.
Zhou, S., Zhuang, X., Rabczuk, T., 2019. Phase-field modeling of fluid-driven dynamic cracking in porous media. Comput. Methods Appl. Mech. Eng. 350, 169–198.
Zienkiewicz, O.C., Humpheson, C., Lewis, R.W., 1975. Associated and non-associated visco-plasticity and plasticity in soil mechanics. Géotechnique 25 (4), 671–689.